Eur. Phys. J. D **4**, 151–158 (1998)

THE EUROPEAN PHYSICAL JOURNAL D

Isotope-selective femtosecond wave packet dynamics: The rare $^{41,41}K_2$ molecule*

S. Rutz[1] and E. Schreiber[2,a]

[1] Universität Rostock, Universitätsplatz 3, 18051 Rostock, Germany
[2] Max-Born-Institut Berlin, Rudower Chaussee 6, 12474 Berlin, Germany

Received: 9 February 1998 / Revised: 15 May 1998 / Accepted: 2 June 1998

Abstract. For the first time, the femtosecond real-time vibrational dynamics of the rare $^{41,41}K_2$ isotope, excited to the electronic $A^1\Sigma^+$ state, could be selectively studied by means of time-resolved three photon ionization. A vibrational period of $T_A^{(41,41)} \cong 500$ fs is determined. Superimposed, a beat structure with a period of 20 ps is observed. A detailed Fourier analysis reveals a strong band of three lines centered around 65.5 cm^{-1}. A significant perturbation of the wave packet caused by spin-orbit coupling of the A and the crossing $b^3\Pi^+$ state is found. This perturbation is the reason for the fast dephasing of the initially generated wave packet within about 10 ps. The spectrogram of the real-time data shows total revivals of the wave packet at 20 ps and 40 ps. Fractional revivals are found for times around 10 ps and 30 ps. Due to high intensity effects a remarkable slightly broadened line at 90 cm^{-1} appears and can be assigned to the wave packet propagation generated in the dimer's ground state by impulsive stimulated Raman scattering. Revivals of this ground state wave packet are found at 17 ps and 34 ps. A comparison with other isotopes of K_2 is given.

PACS. 34.30.+h Intramolecular energy transfer; intramolecular dynamics; dynamics of van der Waals molecules – 82.80.Ms Mass spectrometry (including SIMS, multiphoton ionization and resonance ionization mass spectrometry) – 33.20.Tp Vibrational analysis

1 Introduction

The central idea of the ultrafast spectroscopy of small molecules is the preparation of molecular wave packets followed by the observation of their propagation in real-time [1]. To prepare a wave packet, laser pulses with a large spectral width are required to coherently excite several energy eigenstates with level spacing ΔE_m. In the time domain, this implies that relative to the period $T = 2\pi\hbar/\Delta E_m$ of the molecular motion considered, the duration of the preparation pulse has to be short. Since vibrational periods of small molecules are of the order of $10^{-14} \ldots 10^{-12}$ s, sub-100 fs laser pulses have to be applied to monitor vibrational molecular wave packets in real-time.

Besides few others, mainly the wave packet propagation in photoexcited diatomic [2–4] and triatomic [5–9] molecules have been explored by a variety of techniques. Zewail [2,10,11] and Stolow [12–15] observed the vibrational motion of excited I_2 and Br_2, where the latter is one of the rare examples where more than one isotope was studied. Beyond this, different alkali molecules are treated in great detail [3,4,16–27]. These time-resolved experiments on the alkali dimers used, except [19,20,26], three photon ionization.

The multiphoton ionization allowed us, in particular for the potassium dimer, to isotope-selectively study the induced ultrafast dynamics [1,22,28]. The relatively high density of the dimers in the supersonic molecular beam enabled us to obtain fascinating real-time spectra with high signal-to-noise ratio of the isotopes $^{39,41}K_2$ and $^{39,39}K_2$. It could be shown that the real-time spectroscopy is a highly sensitive method to study excited states and their perturbation owing to crossing states. While in the case of $^{39,39}K_2$ a strong perturbation of the excited electronic $A^1\Sigma_u^+$ state by the $b\,^3\Pi_u$ state *via* spin-orbit coupling was observed, the other isotope however – for the same excitation wavelength $\lambda_{pump} = 833.8$ nm – shows nearly no perturbation. The dynamics of the intersystem crossing processes within the $A^1\Sigma_u^+$–$b\,^3\Pi_u$ system could be analyzed on a femtosecond time-scale for both isotopes. Since the isotope effect observed in the case of $^{39,39}K_2$ and $^{39,41}K_2$ is quite large it is of certain interest, whether similar perturbation phenomena occur in the case of the yet unexplored rare isotope $^{41,41}K_2$. Different experimental

* The experiment presented here has been carried out at the Institut für Experimentalphysik, Freie Universität Berlin, in the laboratories of L. Wöste during the stay of the authors in his group.

[a] e-mail: eschreib@mbi-berlin.de

techniques were used to investigate the A state of K_2. By laser-induced fluorescence, optical-optical double resonance, and Fourier-transform spectroscopy mainly the A state of $^{39,39}K_2$ could be analyzed in great detail [29–31]. For $^{39,41}K_2$ just a few fluorescence lines could be identified [32]. Experimental information on the rare $^{41,41}K_2$ isotope, however, could not be obtained by these experiments. The reason for this is the low concentration of the isotope $^{41,41}K_2$. Since the used potassium contained 93.26% of ^{39}K and 6.73% of ^{41}K (natural abundance), the concentration of the different dimer isotopes behaves as

$$^{39,39}K_2 : {}^{39,41}K_2 : {}^{41,41}K_2 \cong 1 : 0.144 : 0.005. \quad (1)$$

In the case of non-mass-selective detection methods all information on the rare isotope, therefore, is hidden below the strong signals of the other two isotopes. In particular, to the knowledge of the authors till now for no similar prototype system the isotope effect, strongly influencing the photo-induced real-time dynamics, could be studied for the rare isotope.

The real-time experiments of the isotopes $^{39,41}K_2$ and $^{39,41}K_2$ were performed using a modelocked titanium:sapphire laser with only 15 nJ energy per pulse [22], a pulse energy comparably low to the pulse energies available today. These low pulse energies allow a well-defined preparation of a wave packet in the excited state of interest, while laser pulses generated by amplified laser systems (gain: $10^3 \ldots 10^5$) might prepare wave packets in the ground state of the molecule *via* impulsive stimulated Raman scattering as well [33]. Therefore, the use of high-peak power femtosecond laser sources often make the real-time analysis of the molecular dynamics significantly more complex. However, under "low" excitation conditions as used in [22], no signal could be detected for the dimer composed of two rare ^{41}K isotopes. As summarized in Section 2, at first, several improvements of the experimental setup had to be established, to detect the wave packet propagation of the rare isotope $^{41,41}K_2$.

To get even deeper insight into the laser-induced wave packet dynamics, we use the visualization by spectrograms $I(\Delta t, \omega)$. This technique nicely enables the direct observation of the time dependence (Δt) of the different frequency (ω) components originating from the propagating wave packet, including its relative contribution I. Especially, the interplay of the involved frequency groups can be seen at first glance. Revivals, total and fractional [34], will be emphasized in the spectrograms.

This letter is organized in the following way: a brief description and characterization of the used experimental apparatus are presented in Section 2. The presentation of the real-time spectra is given in Section 3.1 followed by an analysis in the frequency domain in Section 3.2. Besides this, the spectrogram technique is applied (Sect. 3.3) providing the total information of the induced wave packet propagation. A comparison with results obtained for two other less rare isotopes is given at the end.

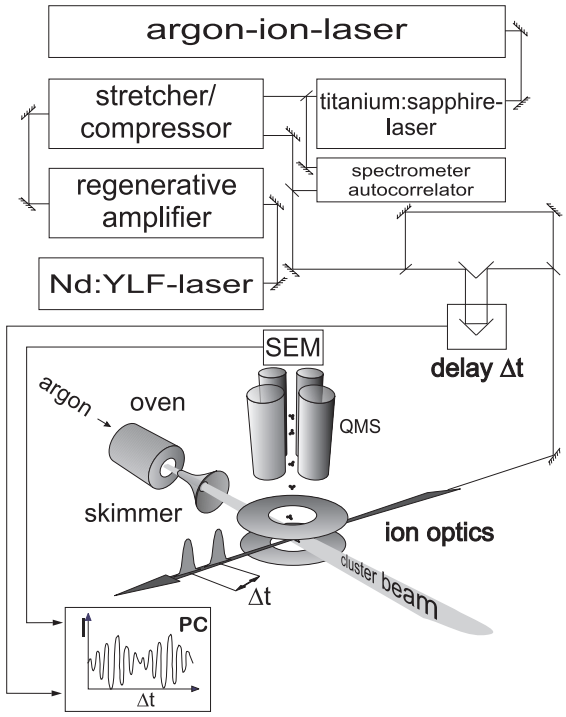

Fig. 1. Experimental setup for femtosecond real-time spectroscopy. The molecular beam is produced in the oven by coexpansion of potassium vapor with argon into vacuum. The beam passes the skimmer and interacts with 70 fs laser pulses, which are generated by a titanium:sapphire laser amplified by a regenerative titanium:sapphire amplifier (using a stretcher/compressor). A pump and probe setup is established by a Michelson-type arrangement introducing a delay time Δt between the pump and the probe pulse. The produced ions are mass-selectively detected by a secondary electron multiplier (SEM) and recorded as a function of the delay time.

2 Experimental

A schematic overview of the experimental setup is given in Figure 1. The production of the molecular beam and its interaction with the femtosecond laser system was realized in a vacuum chamber consisting of two sub chambers. The first sub chamber contained the mechanics to produce the molecular beam while in the second chamber the molecules interacted with the pump and probe laser pulses. The resulting ionic products were detected, using a quadrupole mass spectrometer (QMS) with a secondary electron multiplier (SEM). The mass resolution $m/\Delta m$ of the QMS was approximately 240.

The potassium molecules were generated by radiatively heating pure potassium metal with the natural abundances of the isotopes (see Eq. (1)) and coexpanding the potassium vapor with argon through a 70 μm nozzle. Further details on these principle parts of the used setup are given in [1,22].

The used laser system was based on a regeneratively modelocked titanium:sapphire-laser pumped by an argon-ion-laser. The output of the titanium:sapphire-laser was

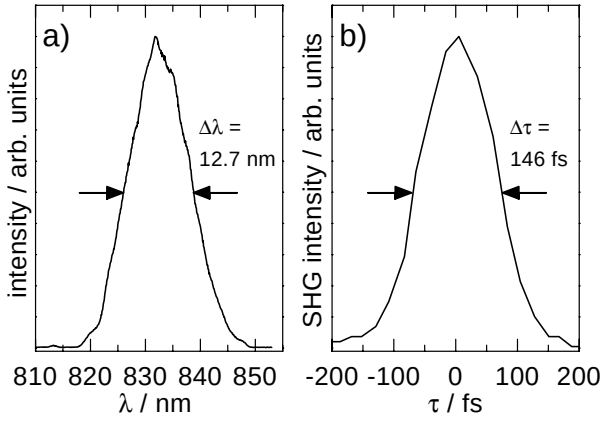

Fig. 2. Spectrum (a) and autocorrelation trace (b) of the amplified titanium:sapphire-laser pulses. Assuming a sech^2 pulse shape, a pulse width $\Delta t = 94$ fs (FWHM) is measured.

a pulse train of laser pulses (pulse duration 70 fs (FWHM), spectral width > 200 cm^{-1}) at a wavelength of 834 nm.

The laser pulses were amplified by a regenerative Amplifier (Quantronix) at 1 kHz. The seed pulses were temporally stretched by a factor of 200 to avoid damage of the titanium:sapphire crystal. The output of the amplifier was recompressed to a pulse duration of about 90 fs with a pulse energy of 460 μJ. An amplification factor of 7.5×10^4 was reached. The autocorrelation trace and the spectrum of the amplified laser are presented in Figure 2.

The amplified laser was aligned through an optical setup to enable pump and probe experiments. The real-time spectrum $I(t)$ of the ion signal I was recorded as a function of the delay time Δt between the pump and the probe laser. We have chosen a typical time step of $\Delta t_{step} = 50$ fs. For this step width the Nyquist critical frequency $\omega_c = 1/(2\Delta t_{step} c) = 333$ cm^{-1} is even larger than four times the expected vibrational frequency $\omega_0 \approx 65$ cm^{-1} [31] of the $A^1\Sigma_u^+$ state. Therefore, an aliasing of realistic frequency components larger than ω_c is negligible in a Fourier analysis since they can not occur.

Compared to the experiments of the other isotopes [22], several improvements of the used experimental setup were necessary to detect this rare isotope.

- The temporal stability of the molecular beam could be drastically increased by a modification of the oven, in particular, a specially formed skiff, used as reservoir for the bulk potassium, was constructed [35].
- The high photon peak intensity of the amplified laser pulses helped to efficiently excite nearly all the rare $^{41,41}K_2$ isotopes present in the molecular beam. One might say, that the use of the amplified titanium:sapphire-laser system, for the first time made possible the mass-selective detection of the very rare isotope's wave packet propagation.
- By carefully aligning the angles in the stretcher/compressor module of the amplifier, pulse widths of below 95 fs for the amplified pulse could be obtained.
- Finally, the quadrupole mass spectrometer's ion optics was adjusted to optimize potassium dimer detection.

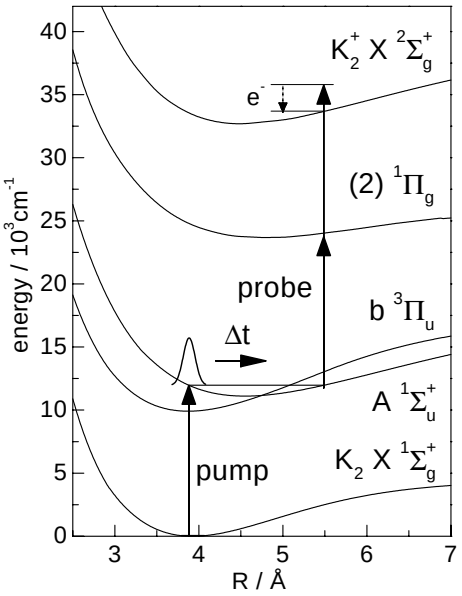

Fig. 3. Excitation scheme for a one-color real-time (3PI) experiment on K_2 (taken from [28]). A wave packet is prepared in the $A^1\Sigma_u^+$ by an ultrashort pump pulse. Its propagation on this PES is probed by a two-photon ionization process. The propagation of the wave packet is perturbed by the $b\,^3\Pi_u$ state. The PES are reconstructed by data from [31,36–38].

3 Results and discussion

In this section we first present the obtained real-time data $I(t)$ of $^{41,41}K_2$ in the time domain (3.1). A detailed analysis in the frequency domain (3.2) follows. Introducing the spectrogram technique (3.3) enables detailed insight into the investigated wave packet dynamics. Especially, it visualizes directly several total and fractional revivals of the laser-induced vibrational wave packets.

3.1 Results in the time domain

The ultrafast wave packet dynamics is investigated by means of a one-color three-photon ionization (3PI) process. Figure 3 illustrates this multiphoton process for K_2. Initially, the dimer is – owing to its generation by adiabatic expansion – in the vibrational state $v'' = 0$ of the electronic ground state $X^1\Sigma_g^+$. Taking into account the known spectroscopic data [30,31,36] of the ground and excited states as well as the Franck–Condon-Principle, the pump pulse prepares in a one-photon step a wave packet on the A state's potential energy surface (PES) close to the inner turning point, energetically centered around $v' = 14$. After a certain delay time Δt this wave packet is probed using two photons trying to ionize the dimer ($K_2^+\ X\,^2\Sigma_g^+$). The electron, separated during the ionization process, takes the excess energy as kinetic energy. A resonant intermediate state ($(2)\,^1\Pi_g$) acts as a spatially small Franck–Condon window. As is seen during the analysis of the real-time spectrum, this state with parity "gerade" acts under these special excitation conditions as a kind of filter, since only

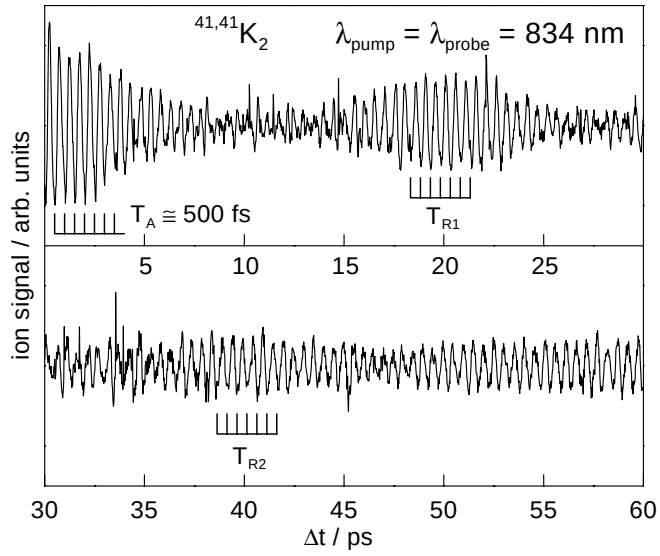

Fig. 4. Real-time spectrum of the isotope $^{41,41}K_2$ excited to its electronic A state using $\lambda_{pump} = \lambda_{probe} = 834$ nm. T_A is the oscillation period of the A state and $T_{R1,2}$ assign the revival times of the photo-induced wave packet.

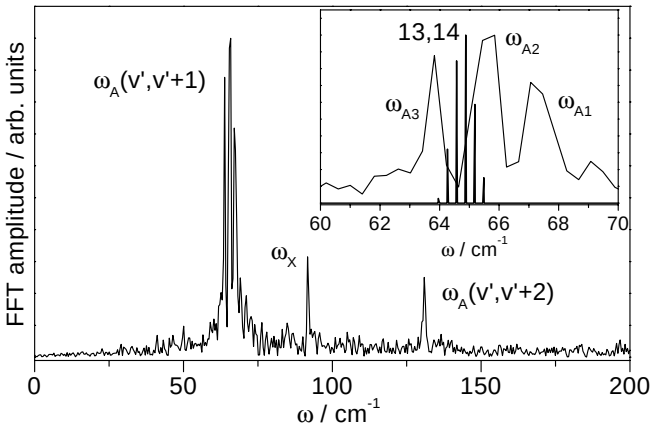

Fig. 5. Fourier spectrum of the real-time data obtained for the isotope $^{41,41}K_2$ excited and ionized with $\lambda_{pump} = \lambda_{probe} = 834$ nm. ω_X can be assigned to the dimer's ground state X. The frequency band at 130 cm^{-1} is owing to dimer modes with $\Delta v' = 2$. The inset shows the first band $\omega_A(v', v'+1)$ with an enlarged scaling. A comparison with line positions calculated on the basis of spectroscopic constants [31] is given.

for a single internuclear separation R (Condon point) of the dimer, the transition can take place from the A state to the ion state. This fact enables the explicit mapping of the wave packet's motion, *i.e.* the signal is expected to come and go periodically as the wave packet travels through this detection window.

The real-time spectrum of $^{41,41}K_2$ is presented in Figure 4. Dominantly, a fast oscillation with $T_A^{(41,41)} \cong 500$ fs is visible in the $^{41,41}K_2$ ion signal. The oscillation's first maximum is reached at a delay time of 250 fs. This periodicity directly mirrors the wave packet dynamics of a vibrational wave packet on the $A^1\Sigma_u^+$ state's PES as similar observed for the lighter isotopes [22] even with different excitation schemes [23]. Since the first maximum's position appears after half a 500 fs cycle (at 250 fs), we can directly identify the Condon point in the probe step of the experiment: it is located at the outer turning point of the A state PES with the Π state Franck–Condon window as described above.

The 500 fs oscillation observed for the first few picoseconds of the real-time spectrum (see Fig. 4), vanishes monotonously, reaching a minimum at a delay time of ≈ 10 ps. At $T_{R1} \cong 20$ ps a first revival of the wave packet occurs. Here, the same 500 fs oscillation as at the zero-of-time is observed. This behavior continues periodically, so that the next revivals are visible at $T_{R2,3} \cong 40$ ps and 60 ps, respectively, resulting in a distinct beat structure. Assuming the $A^1\Sigma_u^+$ state's vibrational levels calculated on the basis of spectroscopic constants (*i.e.* no perturbation with any other electronic state is taken into account) [31] and the appropriate isotopic correction, one would expect the first total revival at a delay time of about 107 ps (see calculated frequencies ω_A in the inset of Fig. 5 and see Eq. (2)). In the next subsections this revival structure is discussed in more detail by means of Fourier transform and a sliding window Fourier transform techniques.

3.2 Frequency analysis

The frequency spectrum of the real-time data, calculated by means of a Fourier transform, is presented in Figure 5. Three frequency components are observed. The most significant feature is a frequency group $\omega_A(v', v'+1)$ centered around 65.5 cm^{-1}. These frequencies correspond to the 500 fs period, observed directly in the real-time spectrum. The frequency group mainly contains three resolved components, $\omega_{A1} = 67.3$ cm^{-1}, $\omega_{A2} = 65.5$ cm^{-1}, and $\omega_{A3} = 63.8$ cm^{-1} (see inset of Fig. 5). These single components are related to the energy level spacings between the vibrational levels in the excited state. As seen in the inset of this figure, the frequencies observed here differ widely from those frequencies which one would expect when exciting a pure anharmonic potential.

As similar observed in the case of the lighter isotopes of K_2 [22] the distribution of the frequency components is broader. Therefore, we must consider that we do not only excite a singlet state, but in particular the coupled electronic system $A^1\Sigma_u^+$–$b^3\Pi_u$ with the pump laser pulse. The result of this excitation can be regarded in terms of energy-shifted vibrational levels in the A state [18,22]. Such an energy shift of vibrational levels influences the respective energy level spacings, which can be seen in the Fourier transform of the real-time data. Additionally, these shifted frequencies ω_{An} lead to a shift of the revival times

$$T_{R(n,n+1)} = \left(c(\omega_{An} - \omega_{An+1})\right)^{-1} \qquad (2)$$

in the wave packet dynamics. The time for the first revival shifts from 107 ps in case of an unperturbed anharmonic oscillator to the value of only 20 ps.

Our earlier investigations of the two isotopes $^{39,39}K_2$ and $^{41,39}K_2$ excited to the coupled $^1\Sigma_u^+$–$b^3\Pi_u$ system [22] demonstrated a similar behavior especially for $^{39,39}K_2$. There, the first revival appeared after 10 ps. A result quite similar to the pattern observed here for $^{41,41}K_2$ is indeed seen in the case of $^{39,39}K_2$ (for comparison see Figs. 7a, b). In the real-time spectrum (Fig. 7a) a beat structure with a period of 10 ps is dominant. Strong line shifts for the vibrational states with $v' = 12, 13$ were deduced from the Fourier spectrum (Fig. 7b). They amount 1.2 cm^{-1} and 2.1 cm^{-1}, respectively. Therefore, frequencies being composed of these two levels are strongly shifted, leading to a beat period of 10 ps instead of 103.6 ps for the unperturbed $^{39,39}K_2$ isotope.There, the frequencies shift such that the wave packet consists of mainly two frequency components although eight states are coherently excited [22]. For the intermediate isotope $^{39,41}K_2$ no drastic shifts of the vibrational energy levels are observed [28], and the first revival appears around 60 ps. Therefore, the perturbation for the heaviest isotope seems to be larger than for $^{39,41}K_2$ and slightly smaller than for the lightest isotope.

The explanation of the 20 ps beat structure in the $^{41,41}K_2$ ion signal (see Fig. 4) is in principle the same as in the case of $^{39,39}K_2$. The exact assignment of the level spacings involved cannot be performed here, because the resolution of the Fourier spectrum is not high enough, especially not as high as in case of the lightest isotope. There, the transient spectrum was recorded up to a delay time of 200 ps with the same time step as used here. In the present experiment we were only able to perform the measurement up to delay times of 60 ps. However, as seen in Figure 5 the comparison of the frequencies measured around 66 cm^{-1} with those calculated on the basis of spectroscopic constants again strongly supports the thesis of a rather strong perturbation of the A state. Besides this, it can be stated that the order of magnitude of the involved level shifts is smaller than in the case of the $^{39,39}K_2$.

Next, it is interesting to focus on the influence of the frequencies ω_{A1}, ω_{A2}, and ω_{A3} on the structure of the real-time spectrum. Classically, we can assign these to the beat periods $T_{B(n,n+1)} = (c(\omega_{An} - \omega_{An+1}))^{-1}$ (with nth frequency component and speed of light c) given by the revival times $T_{R(n,n+1)}$. We get $T_{B(1,2)} = 18.5$ ps and $T_{B(2,3)} = 19.6$ ps. These periods are found as the beat period of 20 ps in Figure 4. As the two (classical) beat times are slightly different, the shape of the beat structure in the real-time spectrum broadens with forthgoing delay time.

The next frequency of interest in Figure 5 is $\omega_A(v', v' + 2) \cong 130$ cm^{-1}. This component with about twice the value of $\omega_A(v', v' + 1)$ is due to induced coherences of vibrational levels with $\Delta v' = 2$. It has to be stated, that owing to the resolution of the measurement, $\omega_A(v', v' + 2)$ might not be a single frequency. A first hint is given by the shoulder visible on the low-frequency side of the line. Further proof is given by the spectrogram technique. In particular, coherences of this type can be seen as fractional revivals in real-time spectra or in the spectrogram [14,23,27]. While in Figure 4 no clear fractional revivals are seen, the sensitive spectrogram technique, however, allows their direct observation. We focus on this point in the next subsection.

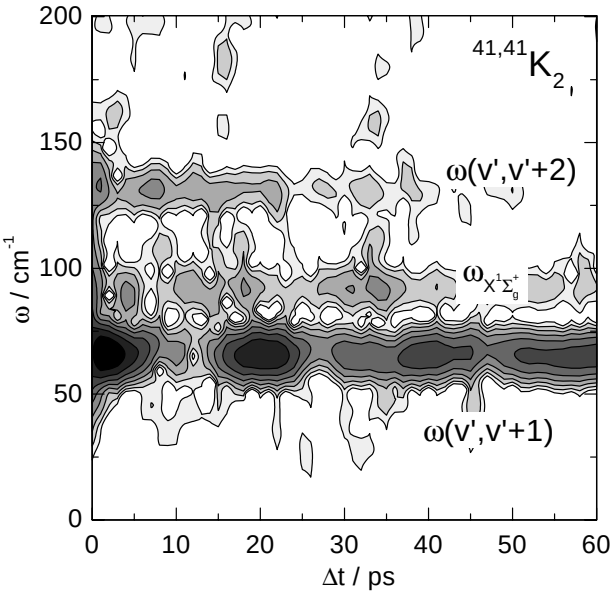

Fig. 6. Spectrogram for $^{41,41}K_2$ excited to its electronic A state; $\lambda_{pump} = \lambda_{probe} = 834$ nm.

The frequency $\omega_X \approx 90$ cm^{-1} can be assigned to the wave packet propagation generated in the ground state by impulsive stimulated Raman scattering. This process becomes more and more probable in K_2, when applying femtosecond laser pulses with high power densities [33]. As discussed for $\omega_A(v', v' + 2)$ this line might as well be composed of at least two components not resolved in the Fourier spectrum. The spectrogram technique again gives a slight proof of this thesis.

3.3 Spectrograms

The real-time spectrum of the molecular vibrational dynamics gives an overview of the temporal evolution of the molecular motion, but allows only a rough estimation of the involved frequencies. On the other hand, the Fourier spectrum presents the frequencies of the laser-induced molecular vibration, but not at all at what certain time which of the frequencies dominate the molecular motion. To obtain deeper insight into the dynamics of the prepared wave packet, it, however, is of great interest to know the temporal evolution of the frequency components, *i.e.* the time Δt when and with what intensity I a certain frequency ω occurs in the real-time spectra. This information can easily be extracted from spectrograms $I(\Delta t, \omega)$ [14,15,28]. For this purpose a procedure is used which first was proposed by Stolow *et al.* to calculate spectrograms of transient data [15]. A sliding-window Fourier transform

$$I(\omega, \Delta t) = \int_0^\infty I(\tau) g(\tau - \Delta t) e^{-i\omega\tau} d\tau \qquad (3)$$

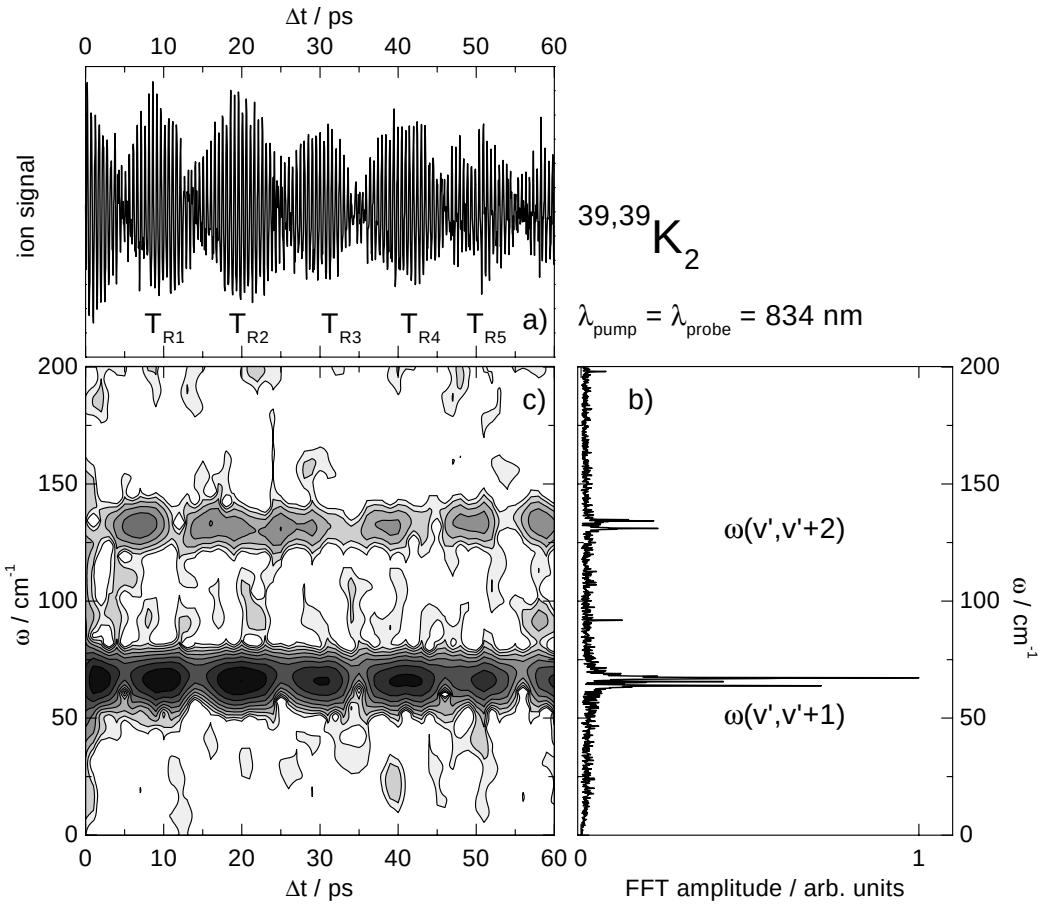

Fig. 7. Data recorded for the isotope $^{39,39}K_2$. The real-time spectrum is shown in part (a), part (b) is the Fourier transform, and in part (c) the spectrogram is illustrated. Note, that with respect to Figure 5 the axis has changed and (b).

is used, where $I(\tau)$ is the real-time ion signal at time τ. For the window function g a Gaussian shape

$$g(\tau) = \exp\left(-\frac{\tau^2}{t_0^2}\right) \tag{4}$$

is chosen with $t_0 = 1$ ps. The Fourier amplitude can be plotted as a function of the delay time Δt and the frequency ω. This enables the direct observation of the time dependence (Δt) of the different frequency (ω) components originating from the propagating wave packet, including their relative contributions I. In particular, the interplay of the frequency groups involved can be seen at a glance. Revivals, total and fractional [34], will be emphasized in the spectrograms. Hence, the introduction of the spectrogram technique for analysis of ultrafast molecular dynamics can be regarded as a highly promising method. Up to now, spectrograms of molecular wave packets have been presented for halogen dimers [14,15] and for alkali dimers [23,27,28]. However, compared to the Fourier analysis, as shown in Figure 5, there is quite a large expense of frequency resolution.

A logarithmic contour plot of the spectrogram is presented in Figure 6. For comparison a spectrogram calculated of the real-time data of $^{39,39}K_2$ is given in Figure 7c. $I(\omega, \Delta t)$ is plotted with increasing gray from white to black. The frequency bands already seen in the frequency spectra (Fig. 5) can now be examined with their temporal evolution. In Figure 6 the main frequency band $\omega_A(v', v'+1)$ (corresponding to $T_A \cong 500$ fs) appears as observed in the real-time spectrum (Fig. 4) every 20 ps. With increasing delay time a broadening of the temporal shape of this frequency is clearly visible. At its revival times, $T_{R1} \cong 20$ ps, $T_{R2} \cong 40$ ps, and $T_{R3} \cong 60$ ps, the wave packet, initially prepared by the pump pulse, runs into total revivals. As pointed out in [22] for the light isotope $^{39,39}K_2$, the fairly short revival time of 20 ps is caused by the spin–orbit coupling between the $A^1\Sigma_u^+$ and $b^3\Pi_u$ states. The related illustration for $^{39,39}K_2$ is given in Figures 7a, c.

The second band, $\omega_A(v', v'+2)$ ($T_{A,2} \cong 250$ fs), caused by coherent superposition of vibrational energy levels with $\Delta v' = 2$, is also visible in Figure 6 every 20 ps between the revival times. Following the ideas of Averbukh and Perel'man [34], the occurrence of the frequency $\omega_A(v', v'+2)$ at half the time of the total revival can be understood as a fractional revival, where the initially prepared wave packet splits into two components. In classical terms, at the times of the fractional revivals these components of the wave packet represent partial wave packets with a phase difference of π with respect to each other.

This leads to the oscillation of the partial wave packets traversing each other.

Hence, in the one-color experiment the ionization step, enhanced by the Franck–Condon window built up by the $(2)^1\Pi$ state, happens two times inside the classical period $T_{A,1}^{41,41} \cong 500$ fs of the A state wave packet. This proof for fractional revivals is not as clear as in case of the lighter isotope (Fig. 7c). There, a clear alternation between $\omega_{A,1}$ and $\omega_{A,2}$ is observable. That structure is more distinct than for $^{41,41}K_2$ because n $^{39,39}K_2$ mainly two frequency components form the band at $\omega_A(v', v'+1)$ (Fig. 7b). In the heavy isotope the wave packet consists of three main components (Fig. 6).

Clearly visible in the spectrogram (Fig. 6) for $^{41,41}K_2$ is the relatively strong amount of frequency components at the ground state's frequency ω_X (compare with $^{39,39}K_2$, Fig. 7c). A weaker revival structure can be seen as well. The frequency ω_X has revivals around 17 ps and 34 ps. Note, that this feature was not detectable in the real-time spectrum but can be identified here with the spectrogram technique.

4 Conclusion

The ultrafast vibrational dynamics of the rare isotope $^{41,41}K_2$, excited to its electronic A state, has been investigated by pump and probe technique. Mass selectivity has been obtained by three photon ionization. Several parameters – in particular, the amplification of the sub-70 fs laser pulses by a factor 7.5×10^4 – of the used experimental setup had to be optimized to enable the detection of a clear signal mirroring the laser-induced wave packet dynamics in the dimer. A clear oscillation with a period of $\cong 500$ fs is visible for the rare isotope over a time interval of more than 60 ps. Total (at 20, 40, and 60 ps) and fractional (at 10, 30, and 50 ps) revivals of the wave packet are nicely resolved and can be assigned straightforward by the application of the spectrogram technique. Moreover, the wave packet dynamics in the ground state with a distinct revival structure (17 ps and 34 ps) could be identified.

These results demonstrate the sensitivity and power of the mass-selective real-time spectroscopy to detect rare isotopes and even analyze their ultrafast dynamics. The spectral information might be improved by measuring the wave packet propagation over a longer time interval, *e.g.* over 200 ps. This should even allow the estimation of energy shifts of the excited vibrational levels caused by spin-orbit coupling of A and crossing b state, as has successfully been performed in the case of the isotope $^{39,39}K_2$. There, the lineshifts could be determined with an accuracy of better than 0.1 cm^{-1}. A comparison of the revival structure found for these two isotopes gives a first hint, that for the isotope $^{41,41}K_2$ excited at $\lambda = 834$ nm is about half of that found for the lighter isotope. The mixed isotope showed a totally different behavior, which is explained by a nearly total missing of the spin-orbit coupling in this excitation region. This drastic differences between the wave packet dynamics of each of the three isotope demonstrates the sensitivity of real-time experiments, presenting clear fingerprints of different isotopes. Besides this, the used technique might be regarded as a stimulating ansatz to use this technique for a controlled isotope separation.

The authors like to thank L. Wöste (Freie Universität Berlin). The experiment, presented here, has been carried out in his laboratories during the stay of the authors in his group. Financial support by the Deutsche Forschungsgemeinschaft DFG within project SFB 337-TP A8 is gratefully acknowledged.

References

1. E. Schreiber, *Springer Tracts in Modern Physics*, Vol. 143 (Springer, Berlin, Heidelberg, 1998).
2. M. Dantus, R. Bowman, A. Zewail, Nature **343**, 737 (1990).
3. T. Baumert, M. Grosser, R. Thalweiser, G. Gerber, Phys. Rev. Lett. **67**, 3753 (1991).
4. S. Rutz, E. Schreiber, in *Ultrafast Phenomena IX*, Vol. 60 of *Springer Series in Chemical Physics*, edited by P. Barbara, W. Knox, G. Mourou, A. Zewail (Springer, Berlin, Heidelberg, 1994), p. 312.
5. K. Kobe, H. Kühling, S. Rutz, E. Schreiber, J. Wolf, L. Wöste, M. Broyer, P. Dugourd, Chem. Phys. Lett. **213**, 554 (1993).
6. T. Baumert, R. Thalweiser, G. Gerber, Chem. Phys. Lett. **209**, 29 (1993).
7. S. Wolf, G. Sommerer, S. Rutz, E. Schreiber, T. Leisner, L. Wöste, Phys. Rev. Lett. **74**, 4177 (1995).
8. B. Reischl, R. de Vivie-Riedle, S. Rutz, E. Schreiber, J. Chem. Phys. **104**, 8857 (1996).
9. H. Ruppe, S. Rutz, E. Schreiber, L. Wöste, Chem. Phys. Lett. **257**, 356 (1996).
10. M. Gruebele, G. Roberts, M. Dantus, R. Bowman, A. Zewail, Chem. Phys. Lett. **166**, 459 (1990).
11. M. Gruebele, A. Zewail, J. Chem. Phys. **98**, 883 (1993).
12. M. Vrakking, I. Fischer, D. Villeneuve, A. Stolow, J. Chem. Phys. **103**, 4538 (1995).
13. I. Fischer, D. Villeneuve, M. Vrakking, A. Stolow, J. Chem. Phys. **102**, 5566 (1995).
14. I. Fischer, M. Vrakking, D. Villeneuve, A. Stolow, Chem. Phys. **207**, 331 (1996).
15. M. Vrakking, D. Villeneuve, A. Stolow, Phys. Rev. A **54**, R37 (1996).
16. J. Papanikolas, R. Williams, P. Kleiber, J. Hart, C. Brink, S. Price, S. Leone, J. Chem. Phys. **103**, 7269 (1995).
17. V. Engel, T. Baumert, C. Meier, G. Gerber, Z. Phys. D **28**, 37 (1993).
18. S. Rutz, S. Greschik, E. Schreiber, L. Wöste, Chem. Phys. Lett. **257**, 365 (1996).
19. H. Schwoerer, P. Pausch, M. Heid, V. Engel, W. Kiefer, J. Chem. Phys. **107**, 9749 (1997).
20. H. Schwoerer, P. Pausch, M. Heid, W. Kiefer, Chem. Phys. Lett. **285**, 240 (1998).
21. R. de Vivie-Riedle, B. Reischl, S. Rutz, E. Schreiber, J. Phys. Chem. **99**, 16829 (1995).
22. S. Rutz, R. de Vivie-Riedle, E. Schreiber, Phys. Rev. A **54**, 306 (1996).
23. S. Rutz, E. Schreiber, Chem. Phys. Lett. **269**, 9 (1997).
24. G. Rodriguez, J. Eden, Chem. Phys. Lett. **205**, 371 (1993).

25. V. Blanchet, M. Bouchene, O. Cabrol, B. Girard, Chem. Phys. Lett. **233**, 491 (1995).
26. L.-E. Berg, M. Beutter, T. Hansson, Chem. Phys. Lett. **253**, 327 (1996).
27. J. Heufelder, H. Ruppe, S. Rutz, E. Schreiber, L. Wöste, Chem. Phys. Lett. **269**, 1 (1997).
28. S. Rutz, Ph.D. thesis, Freie Universität Berlin, Berlin-Dahlem, 1996.
29. A. Ross, P. Crozet, C. Effantin, J. d'Incan, R. Barrow, J. Phys. B **20**, 6225 (1987).
30. A. Lyyra, W. Luh, L. Li, H. Wang, W. Stwalley, J. Chem. Phys. **92**, 43 (1990).
31. G. Jong, L. Li, T.-J. Whang, W. Stwalley, J. Mol. Spectrosc. **155**, 115 (1992).
32. A. Ross, Ph.D. thesis, Université Claude Bernard-Lyon I, Lyon, 1987.
33. R. de Vivie-Riedle, K. Kobe, J. Manz, W. Meyer, B. Reischl, S. Rutz, E. Schreiber, L. Wöste, J. Phys. Chem. **100**, 7789 (1996).
34. I. Averbukh, N. Perel'man, Phys. Lett. A **139**, 449 (1989).
35. F. Kühling, Ph.D. thesis, Freie Universität Berlin, Berlin-Dahlem, 1993.
36. J. Heinze, U. Schühle, F. Engelke, C. Cadwell, J. Chem. Phys. **87**, 45 (1987).
37. W. Meyer, Universität Kaiserslautern (private communication).
38. M. Broyer, J. Chevaleyre, G. Delacrétaz, S. Martin, L. Wöste, Chem. Phys. Lett. **99**, 206 (1983).